catalysts

MDPI

Article

Efficient Heterogeneous Activation of Persulfate by Iron-Modified Biochar for Removal of Antibiotic from Aqueous Solution: A Case Study of Tetracycline Removal

Van-Truc Nguyen [1], Chang-Mao Hung [2], Thanh-Binh Nguyen [2], Jih-Hsing Chang [3], Tsing-Hai Wang [4], Chung-Hsin Wu [5], Yi-Li Lin [6], Chiu-Wen Chen [2,*] and Cheng-Di Dong [2,*]

1 Institute of Marine Science and Technology, National Kaohsiung University of Science and Technology, Kaohsiung 81157, Taiwan; truc1021006@gmail.com
2 Department of Marine Environmental Engineering, National Kaohsiung University of Science and Technology, Kaohsiung 81157, Taiwan; hungcm1031@gmail.com (C.-M.H.); ntbinh179@nkust.edu.tw (T.-B.N.)
3 Department of Environmental Engineering and Management, Chaoyang University of Technology, Taichung 41349, Taiwan; changjh@cyut.edu.tw
4 Department of Chemical Engineering and Materials Science, Yuan Ze University, Zhongli 32003, Taiwan; thwang@saturn.yzu.edu.tw
5 Department of Chemical and Materials Engineering, National Kaohsiung University of Science and Technology, Kaohsiung 80778, Taiwan; wuch@nkust.edu.tw
6 Department of Safety, Health and Environmental Engineering, National Kaohsiung University of Science and Technology, Kaohsiung 82445, Taiwan; yililin@nkust.edu.tw
* Correspondence: cwchen@nkust.edu.tw (C.-W.C.); cddong@nkust.edu.tw (C.-D.D.); Tel.: +886-7-3617141 (ext. 23762); Fax: +886-7-3650548 (C.-D.D.)

Received: 30 October 2018; Accepted: 30 December 2018; Published: 7 January 2019

Abstract: Waste reutilization is always highly desired in the environmental engineering and science community. In this study, Fe-SCG biochar was functionalized by modifying spent coffee grounds (SCG) with magnetite (Fe^{3+}) at 700 °C and applied for the oxidative removal of tetracycline (TC) with the presence of persulfate (PS). The effects of pH, dosage of biochar and sodium persulfate and initial TC concentration on TC degradation were investigated in a batch system. Our results show that higher TC degradation efficiency was obtained at low pH, low initial TC concentration, and at high dosages of PS and biochar. The highest removal efficiency (96%) was achieved by Fe-SCG/PS under the conditions of pH = 2.0, [Fe-SCG] = 2.5 g/L, [PS] = 60 mM and [TC] = 1 mM. The proposed Fe-SCG catalyst could be a promising effective biochar for the remediation of other emerging organic contaminants.

Keywords: spent coffee ground; biochar; tetracycline; sodium persulfate

1. Introduction

Antibiotics are one of the most widely used medicines in preventing microbial infections. A great portion of antibiotic intake cannot be completely metabolized by humans and animals and thus released antibiotics cause serious environmental concerns [1]. According to the sales and distribution data reported by U.S. Food and Drug Administration [2], tetracycline (TC) was the most widely used antibiotic that occupied the highest consumption (42%, ~5,866,588 kg) in 2016. Given the fact that there was an estimated 10–40% of TC being absorbed by the human body, the majority of TC consumed was expected to be discharged into the aquatic environment [3]. Recent field investigations

revealed several alarming facts that high TC concentration was detected in soil (86–199 μg/kg) [4], drinking water (87–97 ng/L) [5], surface water (5.7–8.7 ng/L), ground water (4.4–9.3 ng/L) [6], hospital wastewater (36–1612 ng/L) [7] and municipal wastewater (110–2353 ng/L) [6]. The occurrence of high concentrations of TC further poses an important public health issue, that is, the induction of antibiotic-resistant pathogens [8]. Therefore, an effective and economical treatment solution for TC removal is highly desired by environmental scientists and engineers.

Many technologies have been applied for TC removal, namely adsorption [9], electrochemistry [10], advanced oxidation processes [11] and membrane processes [7]. Among them, adsorption is a cost-effective and fast removal technology [12] and several high-performance adsorbents have been proposed, including activated sludge [13], soil/clays, metal oxides [14], nanocomposite [15] and activated carbon [16]. Recently, biomass-derived adsorbents (biochar) have attracted the interest of scientific community because of their advantages such as low cost, easy operation and are environmentally friendly [17,18]. There have been several successful cases of TC removal by using biochar made from human hair, carbon, rice straw and tea waste [19,20]. Spent coffee grounds (SCG) would be an interesting raw material for synthesis of biochar given its current abundance of about six million tons [21] and 1.2% increase annually [22]. SCG contains various functional groups such as lignin, fatty acids, cellulose, hemicellulose and polyhydroxy polyphenols [23]. Also, SCG has a great portion of lignin structure that is known to be effectively in adsorption application [24]. In fact, SCG has been successfully applied for dyes, heavy metals and organic compounds removal already [23,25].

The performance of biochar is strongly affected by the pyrolysis conditions such as biomass type [19], temperature, pH, reaction time [26] and pyrolysis medium such as pure N_2 and CO_2 [27]. According to the literature [19], temperatures ranging from 300–700 °C would favor biochar preparation by introducing a high surface area and a large amount of micropores. The temperatures above 750 °C could collapse the walls of the micropores and thus decrease the sorption capacity of the biochar as a result of reduced surface area. A biochar synthesized in N_2 condition showed higher adsorption efficiency than those in CO_2 [27]. Recently, iron-modified biochar has been an intense research topic worldwide because it can effectively degrade TC via an oxidation process at the same time. Oladipo et al. [25] compared the TC removal efficiency between the coffee residue biochars with and without the Fe_3O_4 nanoparticle presence. At initial TC concentration of 50 mg/L, pH of 5 and temperature of 25 ± 2 °C with biochar calcined at 300 °C for 2 h, the adsorption capacity of magnetic biochar (285.6 mg/g) was 1.5 times higher than those of conventional biochar (184.5 mg/g). Furthermore, Oladipo et al. [28] synthesized Fe_3O_4-loaded magnetic biochar from chicken bone with a pyrolysis temperature of 500 °C for 2 h. Maximum TC adsorption capacity (63.3 mg/g) was observed at initial TC concentration of 100 mg/L, pH of 10, temperature of 50 °C and biochar of 0.5 g.

Advanced oxidation processes (AOPs) applying highly reactive oxidizing radicals (e.g., hydroxyl radical, sulfate radical, etc.) have been known as an effectively technology for removing organic compounds [29]. Sulfate radicals ($SO_4^{\bullet -}$, E° = 2.6 V) are of particular interest because their half-life is longer than those of hydroxyl radicals ($OH^\bullet$, E° = 2.7 in acidic condition and E° = 1.8 V in alkaline solution) [29]. Sodium persulfate ($Na_2S_2O_8$) has been widely used for sulfate radical generation in AOPs because it is highly chemically stable at room temperature, safe to operate and cost effective [30]. To further enhance TC treatment efficiency of biochar process, oxidants including persulfate (PS) and peroxymonosulfate (PM) were employed. Fe_3O_4 nanoparticle was an effective activator for sulfate radicals, which importantly contribute to the degradation of pollutants. Jafari et al. [31] investigated the TC removal capacity by Fe_3O_4 nanoparticle-coated activated carbon (AC@Fe_3O_4) with the presence of PS. The results indicated that TC degradation by AC@Fe_3O_4 was significantly accelerated from 56% to 81% after 180 min reaction. Typical biochar is less expensive (at least 10 times) than the activated carbon [32]. However, only a few studies have applied the magnetic biochar with PS for TC removal from water environment. Therefore, the aims of this study are to: (i) synthesize of $FeCl_3$ loaded magnetic biochar from SCG, (ii) characterize synthesized biochar, and (iii) assess the TC treatment

efficiency in contaminated water by the prepared biochar with PS under different operating conditions (pH, biochar mass, PS content and initial TC concentration).

2. Results

2.1. Characterization of Biochar

The morphologies of biochar before and after magnetic modification were characterized by a scanning electron microscope (SEM). As shown in Figure 1, there was an evident difference between the surface morphologies of the two materials. The surface of SCG was rather smooth and flat (Figure 1a), whereas Fe-SCG became more heterogeneous and quite rough with several warty protuberances (Figure 1b), which might contribute to the improvement of surface contact area of Fe-SCG, resulting in enhanced adsorption capacity for contaminants. In addition, several spheres appeared on the surface of Fe-SCG (Figure 1d), indicating that iron luster had been formed after loading Fe (III). The energy-dispersive X-ray spectroscope (EDX) images (Figure 1d) demonstrated the iron occurrence (9.27 wt.%) in the Fe-SGC material. The carbon (89.41% and 77.12%) comprised the main composition of both SCG and Fe-SCG respectively, followed by oxygen (10.59% and 13.61%) (Figure 1c,d), which were inherently found in any lignocellulose material [33].

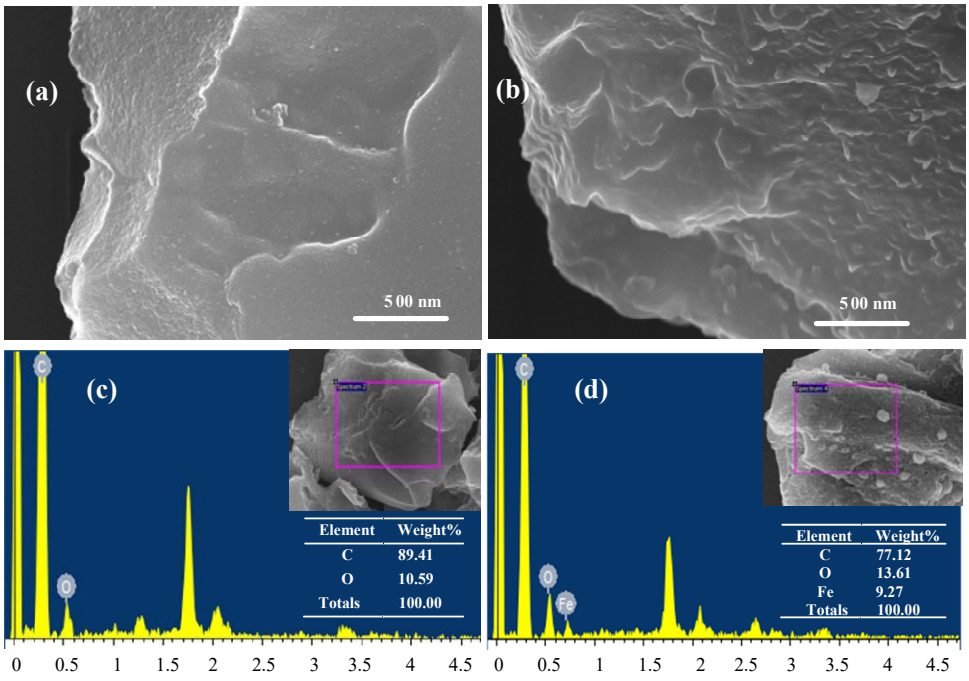

Figure 1. Scanning electron microscope (SEM) images (**a**,**b**) and energy-dispersive X-ray (EDX) spectra (**c**,**d**) for spent coffee grounds (SCG) (left) and Fe-SCG (right).

The Fourier transform-infrared (FTIR) spectra of the SCG and Fe-SCG are displayed in Figure 2a. The band intensities of C–H stretching of aliphatic groups (3000–2800 cm^{-1}) were observed in both the SCG and Fe-SCG. The reductions of the bands for the bending mode of adsorbed water (1627 cm^{-1}), C-C aromatic (1384 cm^{-1}) and aromatic CO-stretching guaiacyl ring in lignin and RCO-O in hemicellulose (1260 cm^{-1}) groups were also observed in the magnetized biochar. This indicated that the lignin in SCG was destroyed during the pyrolysis process [34]. A group of C-O stretching (1085 cm^{-1}) decreased in Fe-SCG due to the degradation of cellulose and hemicellulose [35]. The C–H bending for aromatic (815 cm^{-1}) was obtained in both SCG and Fe-SCG. The degradation of cellulose, lignin and hemicellulose was conducted by pyrolysis, resulting in increased aromatic carbon, which helped to enhance the absorption of biochar [36].

The magnetic characteristics of biochars are depicted in Figure 2b. A magnetic hysteresis loop indicated that the saturation magnetization of SCG and Fe-SCG was 0 and 1.90 emu/g, respectively, demonstrating a good ferromagnetic response of Fe-SCG [31]. It is evident that Fe-SCG can be easily separated from a solution, resulting in avoiding the formation of the secondary pollutants. Both of SCG and Fe-SCG exhibited two distinct peaks at 2θ of 25°, indicating the occurrence of lignocellulose structure, which is in good agreement with the biochars synthesized from the spent coffee ground reported by Ballesteros et al. [24] and Cho et al. [27]. Figure 2c shows Fe_3C mineral with peaks at 29.5°, 40.7°, 42.6°, 45.0° and 49.8°, which were attributed to the (111), (201), (211), (031) and (221) crystal planes (JCPDS 65-2412) was mainly found in Fe-SCG. This might be due to the formation of Fe_3C during the pyrolysis under N_2 condition. Previous studies also reported the same results [27,37].

In addition to the XRD results, X-ray photoelectron spectroscopy (XPS) tests were further employed to investigate the chemical composition of synthesized biochars (Figure 3). Two peaks were observed at 283–288 eV (C 1s) and 530–536 eV (O 1s) in both of SCG and Fe-SCG. The Fe 2p spectra showed two peaks at 710–718 eV and 724–730 eV, which indicated that Fe minerals were formed on the surface of Fe-SCG [38].

The surface of biochar is negatively charged, which facilitates the adsorption of positively charged organics [19]. In this study, both SCG and Fe-SCG were negatively charged with the average zeta potential values of −41.7 mV and −20.9 mV, respectively. These results indicated that the dispersion behavior of SCG was of good stability, while Fe-SCG was of incipient instability, suggesting that it could be easier for Fe-SCG than for SCG to adsorb the pollutants. Furthermore, the average particle size of Fe-SCG (diameter of 520 nm) was smaller than that of SCG (diameter of 680 nm), enhancing the surface area of Fe-SCG.

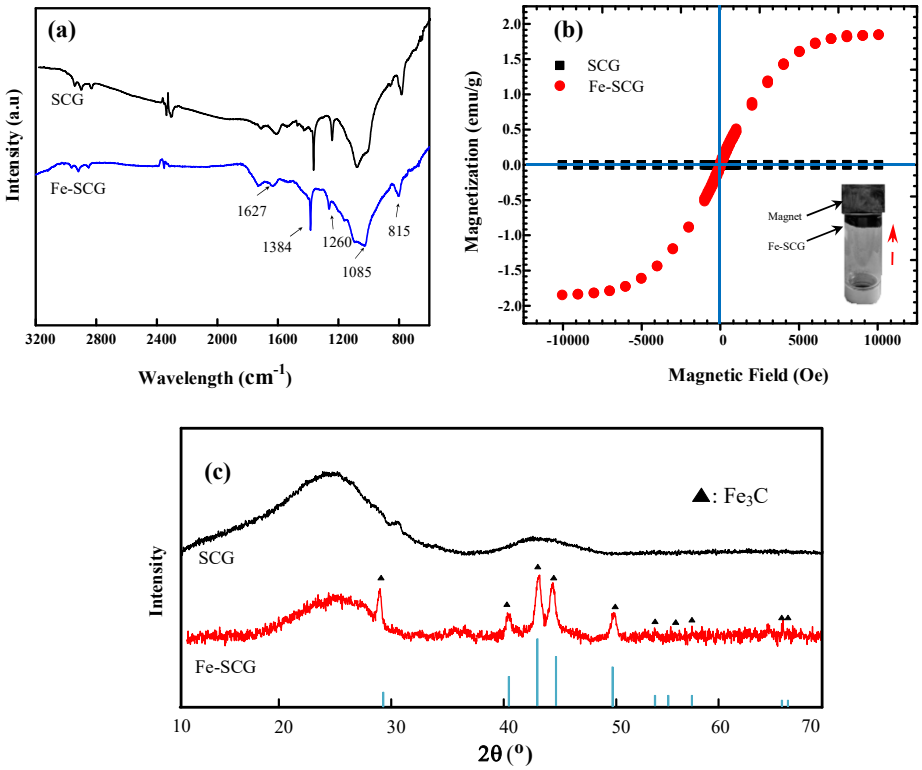

Figure 2. Fourier transform-infrared (FITR) data (**a**), magnetic hysteresis (**b**) and X-ray diffraction (XRD) patterns (**c**) for SCG and Fe-SCG.

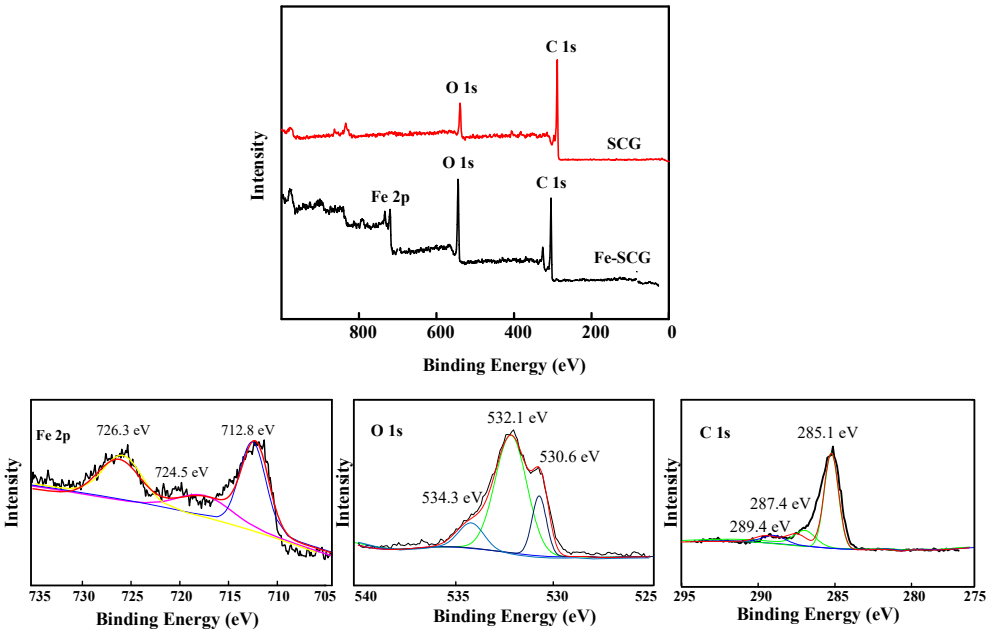

Figure 3. High-resolution X-ray photoelectron spectra (XPS) of SCG and Fe-SCG.

2.2. Adsorption Isotherms

The absorption is the first step of the Fe-SCG/PS process. In this study, Langmuir (Equation (1)) and Freundlich (Equation (2)) adsorption isotherms were obtained under experimental conditions of reaction volume = 50 mL, pH = 2.0, T = 25 °C, agitation = 100 rpm, [Fe-SCG] = 2.5 g/L and [TC] = 0.02–0.2 mM (Figure 4a).

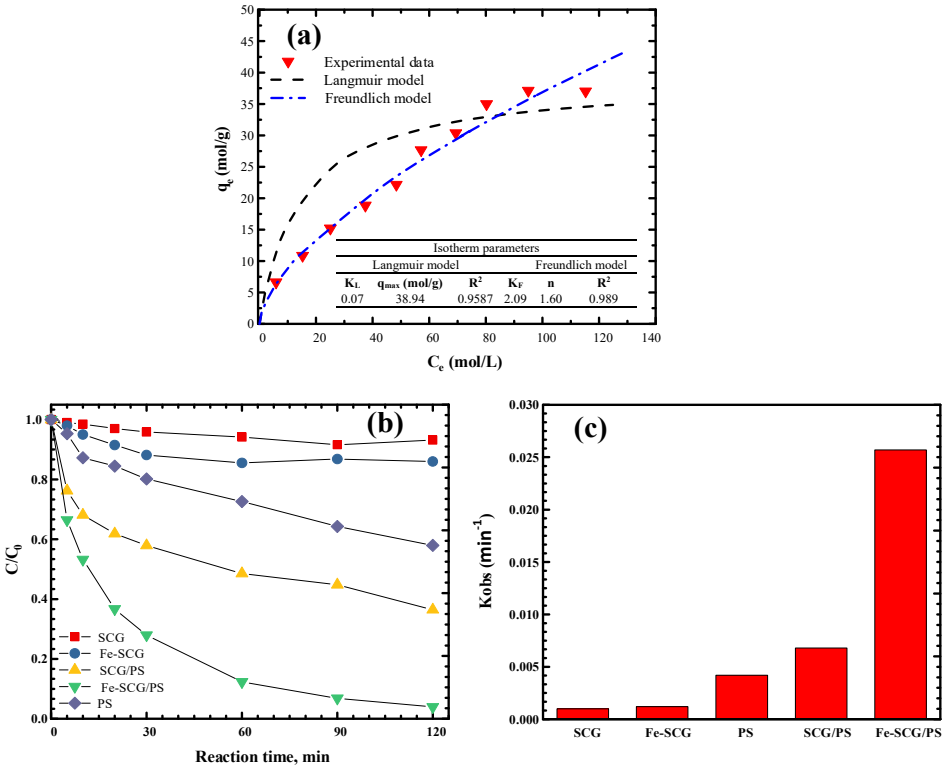

Figure 4. (**a**) Langmuir and Freundlich adsorption isotherms of Fe-SCG; (**b**) TC degradation efficiency and (**c**) degradation rate constant (K_{obs}) of the different processes.

$$\frac{1}{q_e} = \frac{1}{q_{max} K_L C_e} + \frac{1}{q_{max}} \quad (1)$$

$$\log q_e = \log K_F + \frac{1}{n} \log C_e \quad (2)$$

where q_{max} is the maximum monolayer adsorption capacity (mol/g), q_e is the adsorption capacity (mol/g), K_L is the Langmuir constant (L/mol), C_e is equilibrium concentration (mol/L), and K_F (mol/g $(L/mol)^{1/n}$) and 1/n (unitless) are Freundlich constants, respectively. The results show that the equilibrium data of Fe-SCG biochar could well fit both of the two models with high coefficient values ($R^2 > 0.95$). The maximum adsorption capacity of Fe-SCG was determined to be 38.94 mol/g. Compared with other adsorbents [39,40] that have been applied in the removal of TC concentration from aqueous solution, Fe-SCG showed a relatively good adsorption performance.

2.3. Effect of Different Materials on Tetracycline (TC) Degradation

In order to assess the activity of magnetized biochar, TC degradation efficiency using different materials was determined in this study. Experimental conditions used are: reaction volume = 500 mL, pH = 2.0, T = 25 °C, agitation = 500 rpm, [PS] = 60 mM, [TC] = 1 mM, and [biochar] = 2.5 g/L. As depicted in Figure 4b, SCG and Fe-SCG seemed to be not effective in decomposing TC in this case. TC removal efficiency of PS reached 42% after 120 min reaction, indicating PS alone could not completely degrade TC. A higher removal efficiency of 76% was achieved for SCG in the presence of PS. More specifically, TC treatment efficiency (96%) was significantly enhanced when SCG was magnetized with Fe (III) and the support of PS activator. The degradation rate constant (K_{obs}) of Fe-SCG/PS was significantly higher than other processes (Figure 4c).

2.4. Effect of the Initial pH on TC Degradation

The TC degradation by the biochars under different pH conditions was shown in Figure 5a. It can be seen that TC removal efficiency declined as the pH values increased from 2.0–7.0. This finding was agreement with the results reported by Jafari et al. [31]. The degradation rate constant (K_{obs}) at pH 2 was significantly higher than others (Figure 5b). At pH = 2, TC removal reached 97% and subsequently decreased to 31% as pH became neutral. This might be explained by the fact that PS could be easily activated by the iron ions to produce SO_4^{*-} radicals at pH = 2–3. Therefore, the oxidation rate of TC could be enhanced at low pH. Normally, TC formed various functional groups at different pH, namely HTC_2^- at pH more than 9, H_2TC^- at pH 7.6–9, H_3TC at pH 3.4–7.6 and H_4TC^+ at pH less than 3.4 [41,42]. TC existed in cationic forms at pH = 2–3 while the magnetic biochar surface was negatively charged. Thus, high adsorption efficiency occurred under this low pH condition because of electrostatic attraction between TC and the biochar. Moreover, the oxidation process in the magnetic biochar system also enhanced TC removal efficiency of the biochar. Lower TC removals were achieved under higher pH conditions. This could be explained by the fact that the alkaline condition will accelerate the interconversion reactions of SO_4^{*-} radicals to produce $^*OH$ radicals, which has relatively lower oxidation capacity in comparison with SO_4^{*-}. Furthermore, higher pH conditions that could accelerate the precipitation of ferrous ions and hydroxides onto biochar surface significantly contributed to the decreasing TC oxidation. Similar results were also reported in previous studies [31,43]. From the achieved results, pH = 2 seemed to be suitable to apply in further experiments of TC degradation in this study.

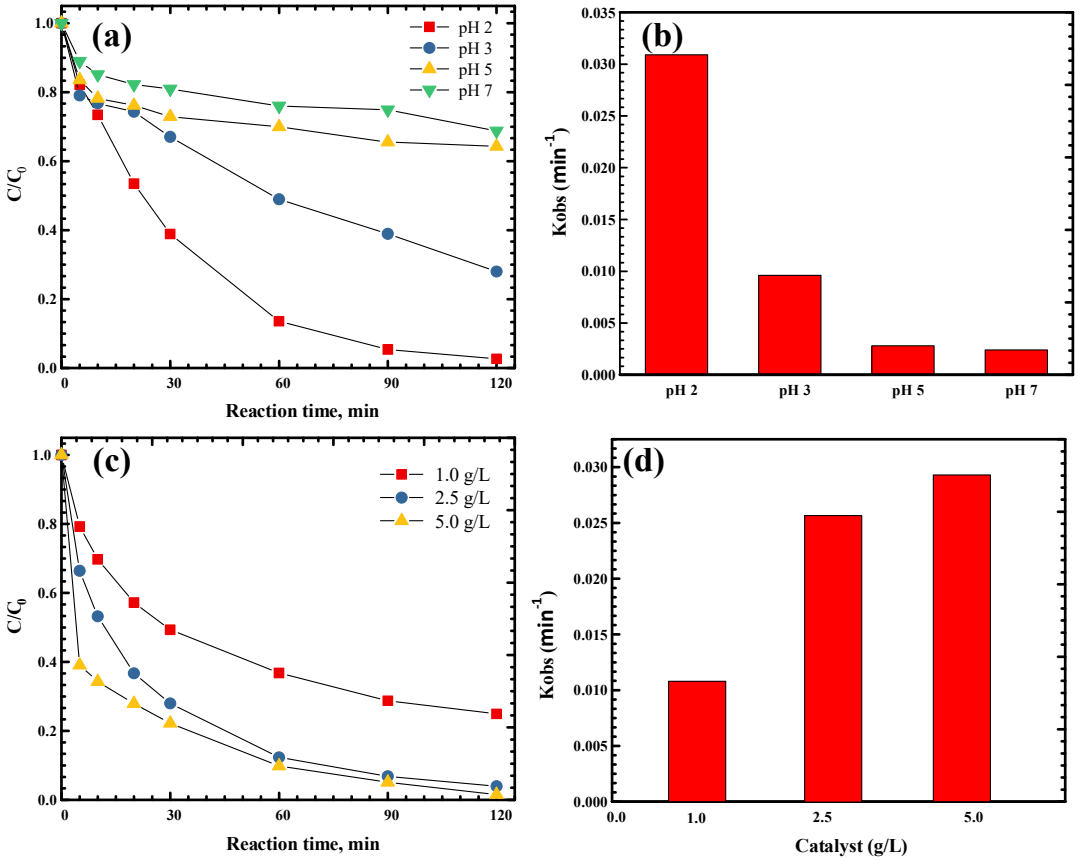

Figure 5. Effects of pH (**a**,**b**) and mass ratios of Fe-SCG catalyst (**c**,**d**) on catalytic reduction of TC.

2.5. Effect of Catalyst Concentrations on TC Degradation

As shown in Figure 5c, TC removal efficiency increased significantly from 75% to 98% when biochar concentration was increased from 1 g/L to 5 g/L within 120 min. Higher dosage led to an increase in the surface area of the biochars which accelerated the contact between TC molecules and the biochar active sites hence improving the adsorption rate of TC [42]. Moreover, the increased biochar dosage also enhanced the production of sulfate radicals leading to a higher removal of TC [44]. The results also showed that the degradation efficiency of TC seemed to slightly improve (from 96% to 98%) after 120 min reaction when the catalyst dosage was increased from 2.5 g/L to 5 g/L. The degradation rate constants (K_{obs}) of Fe-SCG/PS process for both catalyst dosages were likewise insignificantly different (Figure 5d). Considering the economic efficiency, the biochar concentration of 2.5 g/L is, therefore, recommended for large scale application.

2.6. Effect of the Persulfate Activator on TC Degradation

PS plays an important role in TC oxidation because it can produce the sulfate radicals (SO_4^{*-}) that have higher redox potential (2.5–3.1 V) than hydroxyl radicals (1.8–2.7 V). The effect of changing PS concentration on TC removal is shown in Figure 6a,b. It can be observed that the TC removal efficiency and the degradation rate constants (K_{obs}) of the biochars were significantly improved from 60% to 96% and from 0.0079 min^{-1} to 0.0257 min^{-1}, respectively, when PS concentration was increased from 10 mM to 60 mM. The PS molecules could easily reach the biochar surface and react with ferrous ions at higher PS dosage, which was also in accordance with a previous study [29]. At 10 mM PS, TC removal efficiency of Fe-SCG/PS in this study (60%) was lower than that of AC@Fe_3O_4/PS reported by Jafari et al. [31] (65.6%). However, the spent coffee ground (SCG) is more economically feasible than the activated carbon (AC).

2.7. Effect of Initial TC Concentration on TC Degradation

Figure 6c,d present the TC removal efficiency and degradation rate constant (K_{obs}) at varying TC initial concentrations (1.0–2.0 mM). As observed, the highest TC removal (96%) and K_{obs} value (0.0257 min^{-1}) of Fe-SCG were both achieved using 1.00 mM TC concentration. After 120 min reaction, TC removal subsequently reduced from 96% to 68% when TC concentration was increased from 1.0 mM to 2.0 mM. TC would compete with PS in adsorption on the biochar surface when TC content was raised, thereby limiting the generation rate of the sulfate radicals. Furthermore, resistant by-products for PS reaction could also be produced at higher TC concentration [45]. In other words, TC removal would be high under low initial TC concentration because the generation rate of the sulfate radicals was lower than the consumption rate. This study clearly demonstrated that TC degradation by Fe-SCG/PS can reach as high as 90% within 90 min for the case of 1.0 mM initial TC concentration.

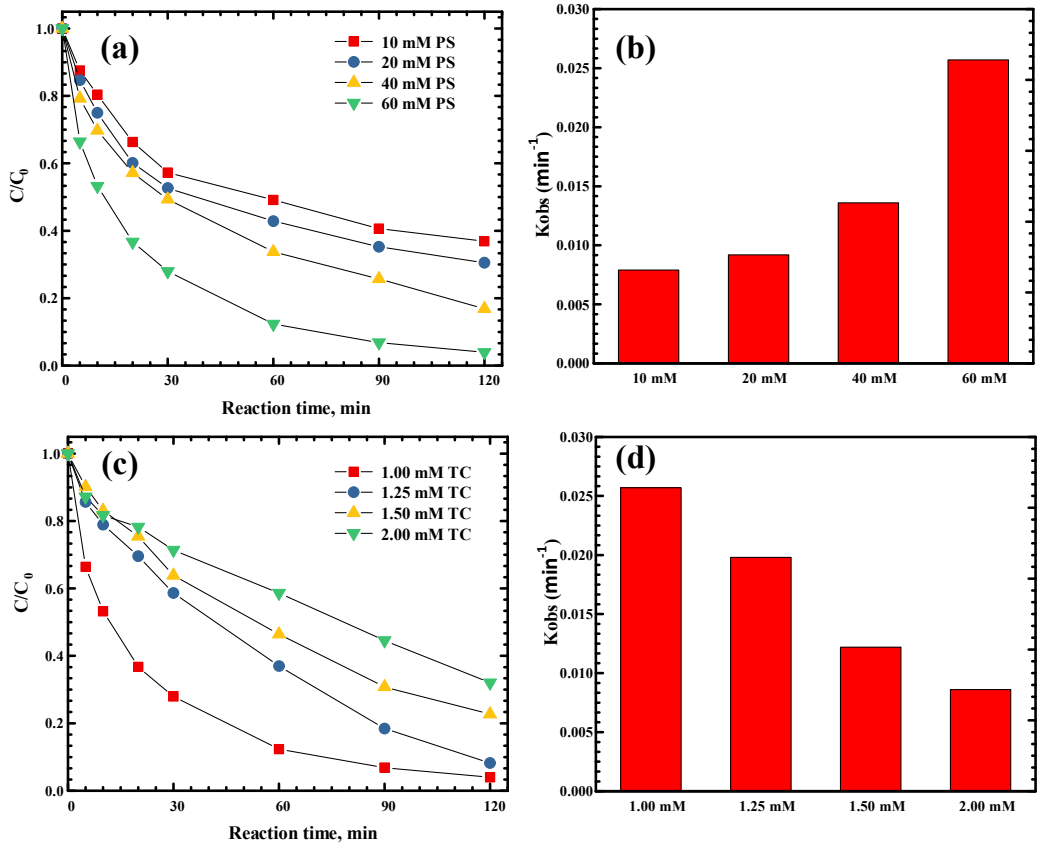

Figure 6. Effects of persulfate (**a**,**b**) and initial TC (**c**,**d**) concentration for catalytic reduction of TC.

2.8. Reaction Mechanism of TC Degradation by Fe-SCG Catalyst in Presence of Persulfate

The reactions for activation of persulfate was summarized and illustrated in Figure 7a. In this study, biochar was magnetized by using Fe (III). The activation mechanism of persulfate by iron-containing catalyst under acidic conditions can be described as follows:

$$Fe^{3+} + S_2O_8^{2-} \rightarrow Fe^{2+} + S_2O_8^{*-} \quad (3)$$

$$Fe^{2+} + S_2O_8^{2-} \rightarrow Fe^{3+} + SO_4^{2-} + SO_4^{*-} \quad (4)$$

In addition, $S_2O_8{}^{*-}$ could be generated by the following reaction:

$$SO_4^{*-} + S_2O_8^{2-} \rightarrow S_2O_8^{*-} + S_2O_4^{2-}. \quad (5)$$

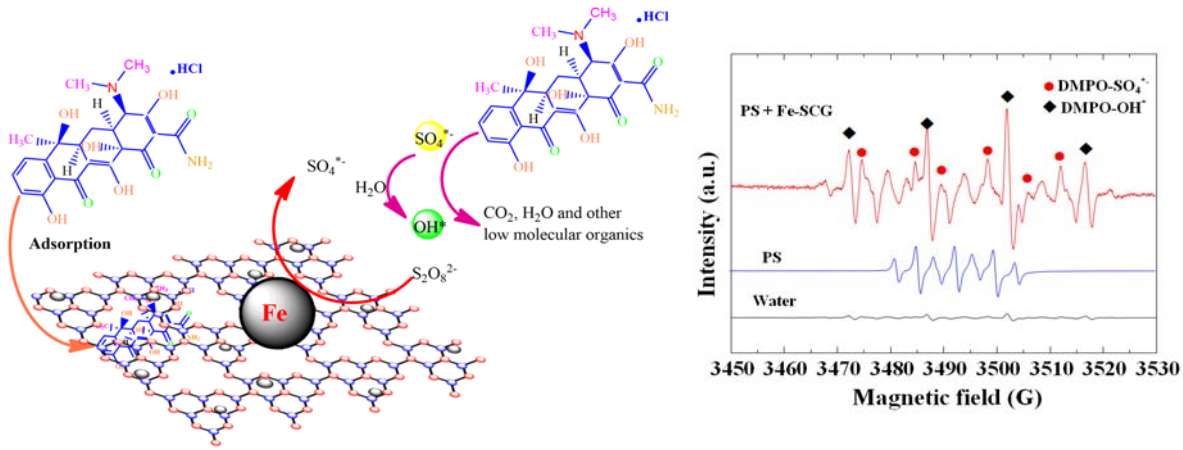

(a) **(b)**

Figure 7. A proposed mechanism of TC degradation by Fe-SCG catalyst in the presence of persulfate (**a**), electron paramagnetic resonance (EPR) spectra generated in the presence of 5,5-dimethylpyrroline-oxide (DMPO) + water, DMPO + PS, DMPO + PS + Fe-SCG (**b**).

However, $S_2O_8^{*-}$ fate was significantly found [46]. Hydroxyl radical can be formed through a reaction between sulfate radical and hydroxyl under highly alkaline condition [47]:

$$SO_4^{*-} + H_2O \rightarrow SO_4^{2-} + OH^* + H^+ \quad (6)$$

$$SO_4^{*-} + OH^- \rightarrow SO_4^{2-} + OH^* \quad (7)$$

In general, the reaction of TC degradation by Fe-SCG catalyst in presence of persulfate was:

$$SO_4^{*-}/OH^* + TC \rightarrow \text{Transformation products} + SO_4^{2-}/OH^- \quad (8)$$

To further gain insights on the production of OH^* and SO_4^{*-} in Fe-SCG/PS system, EPR analysis using 5,5-dimethylpyrroline-oxide (DMPO) as a spin-trapping agent was employed in this study. As presented in Figure 7b, it is clear that no peaks were detected for pure water with the presence of DMPO, indicating that no spins were captured. However, peaks with intensity ratio of 1:2:1:2:1:2:1 that is attributed to 5,5-dimethlprroline-(2)-oxyl-(1) (DMPOX) were identified from the mixture of DMPO and PS. DMPOX is a product of the oxidation of DMPO by PS which is in agreement with previous study [48]. For the mixture of Fe-SCG, DMPO and PS, both DMPO-OH^* and DMPO-SO_4^{*-} were identified. The peaks with intensity ratio of 1:2:2:1 and hyperfine splitting constants of $\alpha_H = \alpha_N =$ 14.9 G could be attributed to DMPO-OH^* [49]. Meanwhile, the pattern of DMPO-SO_4^{*-} (α_N = 13.2 G, α_H = 9.6 G, α_H = 1.48 G, α_H = 0.78 G) is consistent with the findings reported by Shah et al. [50]. In short, the generation of both OH^* and SO_4^{*-} during the catalytic reaction of the Fe-SCG/PS system was confirmed by the EPR results.

3. Materials and Methods

3.1. Iron-Modified Biochar Preparation

Iron-modified biochar was produced according to the process reported by Cho et al. [27]. The spent coffee ground (SCG) was collected from a local coffee shop. In order to remove moisture, the SCG was dried for 3 days at 70 °C; 10 g of SCG was submerged into 100 mL of $FeCl_3$ solution (10 g/L) for 30 min at $FeCl_3$/SCG ratio of 0.1. Water in this mixture was vaporized at 85 °C by using a magnetic stirrer for 2 h. The Fe-soaked SCG was dried in an oven at 50 °C for 24 h. Then, 10 g of the dried Fe-soaked SCG was put in the furnace for the pyrolysis process at 700 °C at a heating rate of 10 °C/min and holding time of 120 min. Pure N_2 flow of 500 mL/min was supplied during the pyrolysis process.

Under the pyrolysis condition with N_2, Fe_3C was generated [51] and attached onto the SCG surface. Iron-modified biochar products were taken out of the furnace when the temperature of the furnace dropped to room temperature. Iron-modified biochars were then cleaned with deionized water several times and dried in the oven at 50 °C for 24 h. Before using in all experiments, the biochars were freeze-dried for 24 h and stored in the oven at 30 °C.

3.2. Chemical Preparation

Tetracycline hydrochloride, methanol (high-performance liquid chromatography (HPLC) grade, ≥99.9%), acetonitrile (HPLC grade, ≥99.9%), oxalic acid dihydrate, sodium persulfate (98%) and ferric chloride hexahydrate (98%) all produced by the Merck group (Merck KGaA, Darmstadt, Germany) were used in this study. Deionized water was used for solution preparation in all experiments. The pH adjustments were conducted using 0.5 M NaOH or and/or 0.5 M HNO_3 [45] supplied by J.T. Baker chemical company (NJ, USA).

3.3. Batch Experimental Design

Five batch experiments were conducted in a 500-mL reactor in this study. Firstly, in order to compare the performance of different materials, the TC removal efficiency by SCG, Fe-SCG, Fe-SCG/PS, PS, and SCG/PS was evaluated at pH = 2, T = 25 °C, TC = 1 mM, PS = 60 mM, content of each material = 2.5 g/L, agitation rate = 500 rpm and PS dose = 1 mL/min. Secondly, evaluation of the TC removal efficiency was conducted at different pH values (2, 3, 4, 5 and 7), biochar = 2.5 g/L, T = 25 °C, TC = 1 mM, PS = 60 mM, agitation rate = 500 rpm and PS dose = 1 mL/min. Next, the effects of changing PS concentration (10, 20, 40 and 60 mM) on the TC removal efficiency were investigated with pH = 2, T = 25 °C, biochar = 2.5 g/L, TC = 1 mM, agitation rate = 500 rpm and PS dose = 1 mL/min. Fourthly, the TC removal efficiency at different biochar contents (1 g/L, 2.5 g/L and 5 g/L) was tested at pH = 2, T = 25 °C, TC = 1 mM, PS = 60 mM, agitation rate = 500 rpm and PS dose = 1 mL/min. Finally, the TC removal efficiency by biochar with different TC concentrations (1.0, 1.25, 1.5 and 2.0 mM) at pH = 2, T = 25 °C, biochar = 2.5 g/L, PS = 60 mM, agitation rate = 500 rpm and PS dose = 1 mL/min. For each experimental period, 1 mL sample was taken out at different reaction times including 0, 5, 10, 20, 30, 60, 90, and 120 min. The solid residues were separated from the filtrate using a 0.22 µm syringe filter. The concentration of tetracycline was analyzed by HPLC. In this study, 1 M potassium iodide (KI) was used as quenching solution.

3.4. Biochar Characteristic Analysis

In order to understand the structure, the surface area and morphological characteristics of biochar were tested by a scanning electronic microscope (SEM, Hitachi S-4800, Tokyo, Japan) with an acceleration voltage of 15 kV. The morphology of catalysts was obtained by an energy-dispersive X-ray spectroscope (EDX, Hitachi S-4800, Tokyo, Japan) at an accelerating voltage of 200 kV. XRD analysis was performed using a Diano-8536 diffractometer equipped with a Cukα radiation source. XPS analyses were carried out using an AXIS Ultra DLD (Kratos Analytical Ltd., Manchester, UK). The magnetic properties of the catalysts were studied using a superconducting quantum interference device magnetometer (MPMS-XL7, Quantum Design, San Diego, CA, USA). The physicochemical properties of the catalysts were also determined by measuring zeta potential while particle size was measured using a Zetasizer Nano ZS90 (Malvern Instruments Ltd., Malvern, Worcestershire, UK). To depict the presence of functional groups attached to biochars, the FTIR spectra data were recorded from 3200 cm^{-1} to 700 cm^{-1} using a FTIR spectrometer (FT-700, Horiba, Kyoto, Japan). To validate the reaction mechanism of the Fe-SCG/PS system, electron paramagnetic resonance (EPR) spectra was recorded by EPR spectrometer (Bruker EMX-10, Karlsruhe, Germany) working at X-band frequency of 9.49–9.88 GHz with power of 8.02 mW.

3.5. Tetracycline Analysis

TC concentration was analyzed using a high performance liquid chromatography system (Chromaster HPLC, Hitachi, Tokyo, Japan) consisting a C/N analysis column (5 μm, 4.6 × 250 mm), a Chromaster 5420 ultraviolet-visible (UV-vis) detector, and a Chromaster 5160 pump. A solution including methanol (≥99.9%, HPLC grade, Merck), acetonitrile (≥ 99.9%, HPLC grade, Merck) and 0.01 M oxalic acid (8:20:72, v/v/v), respectively were used as mobile phase, at a flow rate of 1 mL/min. TC concentration was determined based on the absorbance at 357 nm. Calibration curves were prepared for each experimental batch.

4. Future Research

The findings of this study can demonstrate that the Fe-SCG biochar is an environmental friendly and economically, technically and economically effective absorbent. In future studies, a performance of this biochar for the removal of other emerging contaminants (e.g., antibiotics, pesticides, endocrine disruptors and personal care products) that have gained significant attention in recent years should also be investigated.

5. Conclusions

In this study, we demonstrated that a Fe-SCG/PS system can effectively remove TC in contaminated water through simultaneous involvement of adsorption and oxidation processes. Also, from the mechanism study, we found that TC was mainly degraded through oxidation with SO_4^{*-} radicals. A substantial improvement in degradation efficiency for TC was observed when both Fe-SCG and PS were added. The significant effects of pH, initial TC concentration, and the dosages of PS and catalyst on the TC degradation efficiency were also demonstrated. A high efficiency of more than 96% was obtained by Fe-SCG/PS at pH 2.0, [PS] = 60 mM, [TC] = 1 mM and [Fe-SCG] = 2.5 g/L. These results revealed that Fe-SCG activated PS oxidation can be applied in the future as a promising cost- and environmentally-effective solution for TC removal from aqueous solution in the future.

Author Contributions: V.-T.N. performed the experiments and wrote the paper; C.-M.H. conceived and designed the experiments; T.-B.N. analyzed the data; J.-H.C., T.-H.W., C.-H.W. and Y.-L.L. contributed the reagents/materials/analytical tools; C.-W.C. and C.-D.D. reviewed the final manuscript.

Acknowledgments: The authors would like to thank Marine Research and Development, National Kaohsiung University of Science and Technology, Taiwan, for financially supporting this study under Contract No. 107M01. The authors also thank BM Ensano from University of the Philippines-Diliman for English editing of the final manuscript.

Conflicts of Interest: The authors declare no conflict of interest.

References

1. World Health Organization (WHO). Antimicrobial Resistance: Global Report on Surveillance 2014. Available online: http://apps.who.int/iris/bitstream/handle/10665/112642/9789241564748_eng.pdf;jsessionid=AC57BF3229D37F12700322840FC9902D?sequence=1 (accessed on 25 October 2018).
2. United State Food & Drug Administration (FDA). The 2016 Summary Report on Antimicrobials Sold or Distributed for Use in Food-Producing Animals 2017. Available online: https://www.fda.gov/downloads/forindustry/userfees/animaldruguserfeeactadufa/ucm588085.pdf (accessed on 1 June 2018).
3. Sayğılı, G.A.; Sayğılı, H.; Koyuncu, F.; Güzel, F. Development and physicochemical characterization of a new magnetic nanocomposite as an economic antibiotic remover. *Process Saf. Environ. Prot.* **2015**, *94*, 441–451. [CrossRef]
4. Hamscher, G.; Sczesny, S.; Höper, H.; Nau, H. Determination of persistent tetracycline residues in soil fertilized with liquid manure by high-performance liquid chromatography with electrospray ionization tandem mass spectrometry. *Anal. Chem.* **2002**, *74*, 1509–1518. [CrossRef] [PubMed]

5. Ye, Z.; Weinberg, H.S.; Meyer, M.T. Trace analysis of trimethoprim and sulfonamide, macrolide, quinolone, and tetracycline antibiotics in chlorinated drinking water using liquid chromatography electrospray tandem mass spectrometry. *Anal. Chem.* **2007**, *79*, 1135–1144. [CrossRef] [PubMed]
6. Javid, A.; Mesdaghinia, A.; Nasseri, S.; Mahvi, A.H.; Alimohammadi, M.; Gharibi, H. Assessment of tetracycline contamination in surface and groundwater resources proximal to animal farming houses in Tehran, Iran. *J. Environ. Health Sci. Eng.* **2016**, *14*, 4–8. [CrossRef] [PubMed]
7. Nguyen, T.T.; Bui, X.T.; Luu, V.P.; Nguyen, P.D.; Guo, W.; Ngo, H.H. Removal of antibiotics in sponge membrane bioreactors treating hospital wastewater: Comparison between hollow fiber and flat sheet membrane systems. *Bioresour. Technol.* **2017**, *240*, 42–49. [CrossRef] [PubMed]
8. Christou, A.; Agüera, A.; Bayona, J.M.; Cytryn, E.; Fotopoulos, V.; Lambropoulou, D.; Manaia, C.M.; Michael, C.; Revitt, M.; Schröder, P.; et al. The potential implications of reclaimed wastewater reuse for irrigation on the agricultural environment: The knowns and unknowns of the fate of antibiotics and antibiotic resistant bacteria and resistance genes–A review. *Water Res.* **2017**, *123*, 448–467. [CrossRef] [PubMed]
9. Dong, C.D.; Chen, C.W.; Hung, C.M. Persulfate activation with rice husk-based magnetic biochar for degrading PAEs in marine sediments. *Environ. Sci. Pollut. Res.* **2018**, 1–10. [CrossRef] [PubMed]
10. Yahiaoui, I.; Yahia Cherif, L.; Madi, K.; Aissani-Benissad, F.; Fourcade, F.; Amrane, A. The feasibility of combining an electrochemical treatment on a carbon felt electrode and a biological treatment for the degradation of tetracycline and tylosin–application of the experimental design methodology. *Sep. Sci. Technol.* **2018**, *53*, 337–348. [CrossRef]
11. Heidari, S.; Haghighi, M.; Shabani, M. Ultrasound assisted dispersion of $Bi_2Sn_2O_7$-C_3N_4 Nanophotocatalyst over various amount of zeolite Y for enhanced solar-light photocatalytic degradation of tetracycline in aqueous solution. *Ultrason. Sonochem.* **2018**, *43*, 61–72. [CrossRef]
12. Mohan, D.; Sarswat, A.; Ok, Y.S.; Pittman, C.U., Jr. Organic and inorganic contaminants removal from water with biochar, a renewable, low cost and sustainable adsorbent—A critical review. *Bioresour. Technol.* **2014**, *160*, 191–202. [CrossRef]
13. Neisi, A.; Mohammadi, M.J.; Takdastan, A.; Babaei, A.A.; Yari, A.R.; Farhadi, M. Assessment of tetracycline antibiotic removal from hospital wastewater by extended aeration activated sludge. *Desalin. Water Treat.* **2017**, *80*, 380–386. [CrossRef]
14. Ramesha, G.K.; Kumara, A.V.; Muralidhara, H.B.; Sampath, S. Graphene and graphene oxide as effective adsorbents toward anionic and cationic dyes. *J. Colloid Interface Sci.* **2011**, *361*, 270–277. [CrossRef] [PubMed]
15. Nasseh, N.; Taghavi, L.; Barikbin, B.; Nasseri, M.A. Synthesis and characterizations of a novel $FeNi_3/SiO_2/CuS$ magnetic nanocomposite for photocatalytic degradation of tetracycline in simulated wastewater. *J. Clean. Prod.* **2018**, *179*, 42–54. [CrossRef]
16. Selmi, T.; Sanchez-Sanchez, A.; Gadonneix, P.; Jagiello, J.; Seffen, M.; Sammouda, H.; Celzard, A.; Fierro, V. Tetracycline removal with activated carbons produced by hydrothermal carbonisation of Agave americana fibres and mimosa tannin. *Ind. Crops Prod.* **2018**, *115*, 146–157. [CrossRef]
17. Ramos-Vargas, S.; Alfaro-Cuevas-Villanueva, R.; Huirache-Acuña, R.; Cortés-Martínez, R. Removal of fluoride and arsenate from aqueous solutions by aluminum-modified guava seeds. *Appl. Sci.* **2018**, *8*, 1807. [CrossRef]
18. Jia, P.; Tan, H.; Liu, K.; Gao, W. Removal of methylene blue from aqueous solution by bone char. *Appl. Sci.* **2018**, *8*, 1903. [CrossRef]
19. Ahmad, M.; Rajapaksha, A.U.; Lim, J.E.; Zhang, M.; Bolan, N.; Mohan, D.; Vithanage, M.; Lee, S.S.; Ok, Y.S. Biochar as a sorbent for contaminant management in soil and water: A review. *Chemosphere* **2014**, *99*, 19–33. [CrossRef]
20. Peiris, C.; Gunatilake, S.R.; Mlsna, T.E.; Mohan, D.; Vithanage, M. Biochar based removal of antibiotic sulfonamides and tetracyclines in aquatic environments: A critical review. *Bioresour. Technol.* **2017**, 150–159. [CrossRef] [PubMed]
21. Franca, A.S.; Oliveira, L.S.; Ferreira, M.E. Kinetics and equilibrium studies of methylene blue adsorption by spent coffee grounds. *Desalination* **2009**, *249*, 267–272. [CrossRef]
22. International Coffee Organization (ICO). Coffee Production. 2018. Available online: www.ico.org (accessed on 1 June 2018).

23. Kim, M.S.; Min, H.G.; Koo, N.; Park, J.; Lee, S.H.; Bak, G.I.; Kim, J.G. The effectiveness of spent coffee grounds and its biochar on the amelioration of heavy metals-contaminated water and soil using chemical and biological assessments. *J. Environ. Manag.* **2014**, *146*, 124–130. [CrossRef]
24. Ballesteros, L.F.; Teixeira, J.A.; Mussatto, S.I. Chemical, functional, and structural properties of spent coffee grounds and coffee silverskin. *Food Bioproc. Technol.* **2014**, *7*, 3493–3503. [CrossRef]
25. Oladipo, A.A.; Abureesh, M.A.; Gazi, M. Bifunctional composite from spent "Cyprus coffee" for tetracycline removal and phenol degradation: Solar-Fenton process and artificial neural network. *Int. J. Biol. Macromol.* **2016**, *90*, 89–99. [CrossRef] [PubMed]
26. Jia, Y.; Shi, S.; Liu, J.; Su, S.; Liang, Q.; Zeng, X.; Li, T. Study of the effect of pyrolysis temperature on the Cd^{2+} adsorption characteristics of biochar. *Appl. Sci.* **2018**, *8*, 1019. [CrossRef]
27. Cho, D.W.; Yoon, K.; Kwon, E.E.; Biswas, J.K.; Song, H. Fabrication of magnetic biochar as a treatment medium for As (V) via pyrolysis of $FeCl_3$-pretreated spent coffee ground. *Environ. Pollut.* **2017**, *229*, 942–949. [CrossRef] [PubMed]
28. Oladipo, A.A.; Ifebajo, A.O.; Nisar, N.; Ajayi, O.A. High-performance magnetic chicken bone-based biochar for efficient removal of rhodamine-B dye and tetracycline: Competitive sorption analysis. *Water Sci. Technol.* **2017**, *76*, 373–385. [CrossRef] [PubMed]
29. Matzek, L.W.; Carter, K.E. Activated persulfate for organic chemical degradation: A review. *Chemosphere* **2016**, *151*, 178–188. [CrossRef] [PubMed]
30. Adewuyi, Y.G.; Sakyi, N.Y. Simultaneous absorption and oxidation of nitric oxide and sulfur dioxide by aqueous solutions of sodium persulfate activated by temperature. *Ind. Eng. Chem. Res.* **2013**, *52*, 11702–11711. [CrossRef]
31. Jafari, A.J.; Kakavandi, B.; Jaafarzadeh, N.; Kalantary, R.R.; Ahmadi, M.; Babaei, A.A. Fenton-like catalytic oxidation of tetracycline by AC@Fe_3O_4 as a heterogeneous persulfate activator: Adsorption and degradation studies. *J. Ind. Eng. Chem.* **2017**, *45*, 323–333. [CrossRef]
32. Creamer, A.E.; Gao, B.; Zhang, M. Carbon dioxide capture using biochar produced from sugarcane bagasse and hickory wood. *Chem. Eng. J.* **2014**, *249*, 174–179. [CrossRef]
33. Pap, S.; Knudsen, T.Š.; Radonić, J.; Maletić, S.; Igić, S.M.; Sekulić, M.T. Utilization of fruit processing industry waste as green activated carbon for the treatment of heavy metals and chlorophenols contaminated water. *J. Clean. Prod.* **2017**, *162*, 958–972. [CrossRef]
34. Hao, F.; Zhao, X.; Ouyang, W.; Lin, C.; Chen, S.; Shan, Y.; Lai, X. Molecular structure of corncob-derived biochars and the mechanism of atrazine sorption. *Agron. J.* **2013**, *105*, 773–782. [CrossRef]
35. Yang, H.; Yan, R.; Chen, H.; Lee, D.H.; Zheng, C. Characteristics of hemicellulose, cellulose and lignin pyrolysis. *Fuel* **2007**, *86*, 1781–1788. [CrossRef]
36. Uchimiya, M.; Wartelle, L.H.; Klasson, K.T.; Fortier, C.A.; Lima, I.M. Influence of pyrolysis temperature on biochar property and function as a heavy metal sorbent in soil. *J. Agric. Food Chem.* **2011**, *59*, 2501–2510. [CrossRef] [PubMed]
37. Hu, Y.; Jensen, J.O.; Zhang, W.; Martin, S.; Chenitz, R.; Pan, C.; Xing, W.; Bjerrum, N.J.; Li, Q. Fe_3C-based oxygen reduction catalysts: Synthesis, hollow spherical structures and applications in fuel cells. *J. Mater. Chem. A* **2015**, *3*, 1752–1760. [CrossRef]
38. Domínguez, C.; Perez-Alonso, F.J.; Salam, M.A.; Al-Thabaiti, S.A.; Peña, M.A.; Barrio, L.; Rojas, S. Effect of the N content of Fe/N/graphene catalysts for the oxygen reduction reaction in alkaline media. *J. Mater. Chem. A* **2015**, *3*, 24487–24494. [CrossRef]
39. Chen, Y.; Wang, F.; Duan, L.; Yang, H.; Gao, J. Tetracycline adsorption onto rice husk ash, an agricultural waste: Its kinetic and thermodynamic studies. *J. Mol. Liq.* **2016**, *222*, 487–494. [CrossRef]
40. Liu, P.; Liu, W.J.; Jiang, H.; Chen, J.J.; Li, W.W.; Yu, H.Q. Modification of bio-char derived from fast pyrolysis of biomass and its application in removal of tetracycline from aqueous solution. *Bioresour. Technol.* **2012**, *121*, 235–240. [CrossRef]
41. Palominos, R.A.; Mondaca, M.A.; Giraldo, A.; Peñuela, G.; Pérez-Moya, M.; Mansilla, H.D. Photocatalytic oxidation of the antibiotic tetracycline on TiO_2 and ZnO suspensions. *Catal. Today* **2009**, *144*, 100–105. [CrossRef]
42. Marzbali, M.H.; Esmaieli, M.; Abolghasemi, H.; Marzbali, M.H. Tetracycline adsorption by H_3PO_4-activated carbon produced from apricot nut shells: A batch study. *Process Saf. Environ. Prot.* **2016**, *102*, 700–709. [CrossRef]

43. Fujioka, N.; Suzuki, M.; Kurosu, S.; Kawase, Y. Linkage of iron elution and dissolved oxygen consumption with removal of organic pollutants by nanoscale zero-valent iron: Effects of pH on iron dissolution and formation of iron oxide/hydroxide layer. *Chemosphere* **2016**, *144*, 1738–1746. [CrossRef]
44. Khataee, A.; Salahpour, F.; Fathinia, M.; Seyyedi, B.; Vahid, B. Iron rich laterite soil with mesoporous structure for heterogeneous Fenton-like degradation of an azo dye under visible light. *J. Ind. Eng. Chem.* **2015**, *26*, 129–135. [CrossRef]
45. Safari, G.H.; Nasseri, S.; Mahvi, A.H.; Yaghmaeian, K.; Nabizadeh, R.; Alimohammadi, M. Optimization of sonochemical degradation of tetracycline in aqueous solution using sono-activated persulfate process. *J. Environ. Health Sci. Eng.* **2015**, *13*, 76–90. [CrossRef] [PubMed]
46. Liu, H.; Bruton, T.A.; Doyle, F.M.; Sedlak, D.L. In situ chemical oxidation of contaminated groundwater by persulfate: Decomposition by Fe(III)-and Mn(IV)-containing oxides and aquifer materials. *Environ. Sci. Technol.* **2014**, *48*, 10330–10336. [CrossRef] [PubMed]
47. Furman, O.S.; Teel, A.L.; Watts, R.J. Mechanism of base activation of persulfate. *Environ. Sci. Technol.* **2010**, *44*, 6423–6428. [CrossRef] [PubMed]
48. Lee, H.; Lee, H.J.; Jeong, J.; Lee, J.; Park, N.B.; Lee, C. Activation of persulfates by carbon nanotubes: Oxidation of organic compounds by nonradical mechanism. *Chem. Eng. J.* **2015**, *266*, 28–33. [CrossRef]
49. Nguyen, T.B.; Huang, C.P.; Doong, R.-A. Photocatalytic degradation of bisphenol A over a $ZnFe_2O_4/TiO_2$ nanocomposite under visible light. *Sci. Total Environ.* **2019**, *646*, 745–756. [CrossRef] [PubMed]
50. Shah, N.S.; Khan, J.A.; Sayed, M.; Khan, Z.U.; Ali, H.S.; Murtaza, B.; Khan, H.M.; Imran, M.; Muhammad, N. Hydroxyl and sulfate radical mediated degradation of ciprofloxacin using nano zerovalent manganese catalyzed $S_2O_8^{2-}$. *Chem. Eng. J.* **2019**, *356*, 199–209. [CrossRef]
51. Kramm, U.I.; Herrmann-Geppert, I.; Fiechter, S.; Zehl, G.; Zizak, I.; Dorbandt, I.; Schmeißer, D.; Bogdanoff, P. Effect of iron-carbide formation on the number of active sites in Fe–N–C catalysts for the oxygen reduction reaction in acidic media. *J. Mater. Chem. A* **2014**, *2*, 2663–2670. [CrossRef]